Journal of Inorganic Biochemistry 191 (2019) 194–202

Contents lists available at ScienceDirect

Journal of Inorganic Biochemistry

journal homepage: www.elsevier.com/locate/jinorgbio

Triphenyltin(IV) acylhydrazone compounds: Synthesis, structure and bioactivity

Xicheng Liu*,[1], Yanhua Tang[1], Xiangdong He, Xingxing Ge, Jiao Liu, Xiaoyu Meng, Mingxiao Shao, Yingmin Jin, Laijin Tian*, Zhe Liu*

Institute of Anticancer Agents Development and Theranostic Application, The Key Laboratory of Life-Organic Analysis and Key Laboratory of Pharmaceutical Intermediates and Analysis of Natural Medicine, School of Chemistry and Chemical Engineering, Qufu Normal University, Qufu 273165, China

ARTICLE INFO

Keywords:
Triphenyltin(IV)
Acylhydrazone
Antitumor

ABSTRACT

Four new triphenyltin(IV) acylhydrazone compounds of the type $Ph_3SnCH_2CH_2CONHN=R$ (where Ph = phenyl; R = isopropyl, isobutyl, cyclopentyl and cyclooctyl) were synthesized and characterized by elemental analysis, infrared spectrum (IR), nuclear magnetic resonance spectrum (NMR) and mass spectrum (MS). The crystal structures were determined and showed that tin atoms were four-coordinated and adopted a pseudo-tetrahedron configuration. Tin(IV) compounds show excellent bovine serum albumin (BSA) binding properties, and can oxidize nicotinamide-adenine dinucleotid (NADH) to generate reactive oxygen species (ROS), which inducing apoptosis effectively. Bioassay results indicated that tin(IV) compounds have stronger cytotoxic activity against A549 human lung cancer cells compared with *cis*-platin used clinically, and showing some selectivity.

1. Introduction

Since Rosenberg et al. found *cis*-platin has antitumor activity in 1969, the medicinal properties of metal complexes have attracted wide attention and opened up a new field of research [1–4]. Now, platinum complexes have widely used to treat various cancer [5]. The treatment with platinum-based drugs or platinum-related drugs accounted for > 50% among all chemotherapy regiments. However, widely used it is today, the platinum antitumor drugs also show some of the increasingly prominent problem-severe side effects [6], which urge researchers to seek the alternative antitumor drugs with more efficient, better targeted, and the antitumor mechanism different from platinum drugs [7]. Among these, organotin compound is one of the most active metal organic compound in the last few decades. A large number of organotin compounds have shown higher antitumor activity than the widely used *cis*-platin antitumor drugs by experiments in vitro [8–13].

Schiff base mainly refers to series of organic compounds containing the imide or methylamine group (−RC═N−), which were usually condensed by amine and active carbonyl including the type of amino acids, thiosemicarbazones, shrinkage amine, heterocyclic, hydrazone etc. [14]. Schiff base has the unique medicinal effect in antibacterial, bactericidal, antitumor and anti-virus [15]. And also, Schiff base has good coordination ability with transition metal using nitrogen and oxygen atoms inside the group [16]. More importantly, because of the special structure, Schiff base is close to the real situation of biological system and suitable for the simulation study of life system, which have attracted more and more attention in recent years [17]. Acylhydrazone derivatives are a special class of Schiff base compounds, which are formed by the condensation of hydrazine and aldehydes or ketones. The structure is characterized by the presence of −CO−NH−N═C− fragment in the molecule. The *p*-π conjugation existed in the fragment of amino group, the carbonyl group and the amino group enhance the stability of compounds. The bigger conjugate system increase electron liquidity of intramolecular and give such compounds special activity [18].

Organotin compounds have strong biological toxicity, which was in relation to their organotin parts and the types of ligands. The low molecular weight organotin can seriously damage the immune system. The more numbers of alkyl substituents, the stronger of the hydrophobic, and the greater of compound's toxicity [19]. However, recent research has shown that the toxicity will decrease when the numbers of alkyl substituents increased to a certain extent, or increasing the carbon chain length connected with tin atom and the volume of compounds [20]. Given these, in this article, acylhydrazone units condensed by alkyl ketones and hydrazines were introduced into the alkyl substituents to increase the carbon chain length and the volume of

* Corresponding authors.
E-mail addresses: chemlxc@163.com (X. Liu), tianlaijin@163.com (L. Tian), liuzheqd@163.com (Z. Liu).
[1] X. C. Liu and Y. H. Tang have equivalent contribution.

https://doi.org/10.1016/j.jinorgbio.2018.11.011
Received 27 June 2018; Received in revised form 17 November 2018; Accepted 17 November 2018
Available online 24 November 2018
0162-0134/

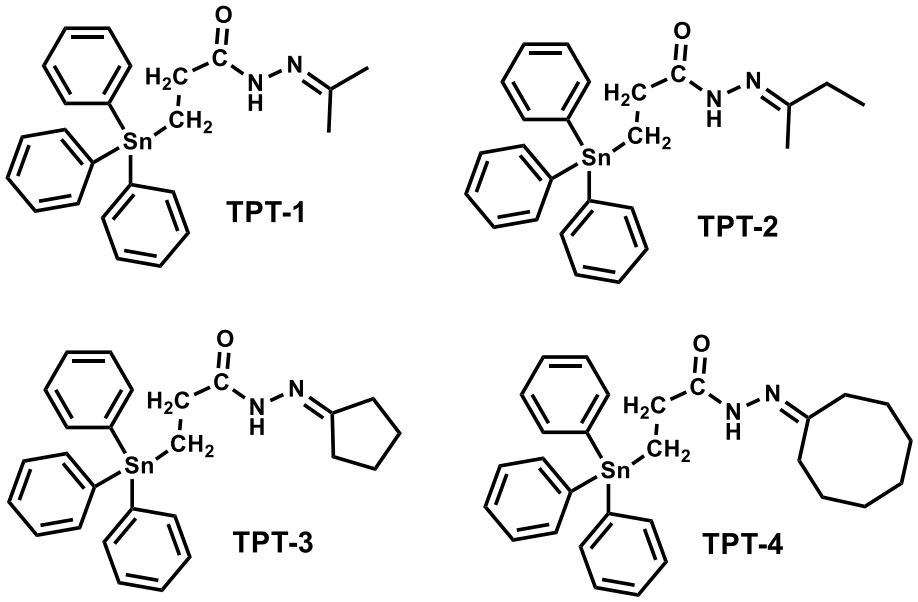

Fig. 1. The structure of as-synthesized triphenyltin(IV) compounds **TPT-1–TPT-4**.

triphenyltin(IV) compounds (Fig. 1), which enhancing the lipid solubility, reducing the toxicity and improving antitumor activity of tin compounds. The antitumor activities of **TPT-1–TPT-4** were evaluated against A549 human lung cancer cells by 3-(4,5-dimethylthiazol-2-yl)-2,5-diphenyltetrazolium bromide (MTT) assay, and *cis*-platin was used as the positive and negative control for the cytotoxicity study in vitro. The anti-cancer mechanism was further studied by bovine serum albumin (BSA) interaction, reaction with nicotinamide-adenine dinucleotid (NADH), apoptosis assay, cell cycle analysis and reactive oxygen species (ROS) production.

2. Results and discussion

Tin(IV) compounds were obtained with cheap starting materials and a simple synthesis process. The prepared tin(IV) compounds and synthetic routes are summarized in Fig. 1 and Scheme 1, respectively. As-synthesized tin(IV) compounds were fully characterized by elemental analysis, IR, ^{1}H NMR, ^{13}C NMR, ^{119}Sn NMR and MS (ESI Figs. S1–S3). All the analytical data are consistent with the proposed structures.

2.1. Crystal structures

Single crystals of **TPT-1**, **TPT-3** and **TPT-4** suitable for X-ray diffraction analysis were obtained by slow diffusion of hexane into a saturated dichloromethane solution of the compounds. The three X-ray crystal structures are shown in Fig. 2, the crystallographic data and the selected bond lengths, bond angles are listed in Tables 1 and 2, respectively. Except for **TPT-4**, one crystal unit cell contains two molecules for **TPT-1** and **TPT-3**. In all of these compounds, the coordination geometry around tins are described as pseudo-tetrahedron with the bond angels of C—Sn—C changed from 101.8(5)° to 119.3(5)°. Because of the high electron density on tin atoms induced by the excellent electron donor characteristic of phenyl, the O(1) of the acylhydrazone group did not coordinate with Sn(1), which are reflected in the long separation distance of Sn(1)-O(1) (2.913(4), 2.855(3) and 3.412(5) Å for **TPT-1**, **TPT-3** and **TPT-4**, respectively, which is longer than the usual Sn—O coordination bond (2.3–2.6 Å)) [21]. The result is consistent with the analysis of the elastic vibration frequency of the carbonyl group in IR (> 1650 cm^{-1}) [22,23]. The ^{119}Sn NMR chemical shift and $^{1}J(^{119}\text{Sn}\text{-}^{13}\text{C})$ values may also be used to give tentative indications of the environment around tin atoms [24]. As shown in ESI Fig. S2, the ^{119}Sn NMR and $^{1}J(^{119}\text{Sn}\text{-}^{13}\text{C})$ values of tin(IV) compounds indicate that the tin atom is four-coordinated and carbonyl does not coordinate to tin in $CDCl_3$ solution. And also, the values of ^{13}C (C═O) were almost same for selected **TPT-4** and the corresponding non-metallated acylhydrazone monomer (ESI Figs. S4 and S5), which further confirmed the conclusion.

It is worth mentioning that the distance of Sn(1)-O(1) are shorter than the van der Waals radius (3.78 Å) [25] for all triphenyltin(IV) compounds, showing that some interaction still exist between Sn(1) and O(1), which play a certain role in the distortion of tetrahedral configuration. The intramolecular hydrogen bonds between O(1) and hydrogen atom of N(1) existed in all compounds. Among these, **TPT-4** form dimer (ESI Fig. S6b) using intermolecular hydrogen bonds, while **TPT-1** and **TPT-3** form one-dimensional (1D) chain structures (Fig. 3 and ESI Fig. S6a) [26].

2.2. In vitro cytotoxicity

The antitumor activities of compound **2** (raw material, triphenyltin (IV) compound substituted by hydrazine carbonyl), **TPT-1–TPT-4** were evaluated against A549 human lung cancer cells by MTT assay, and *cis*-platin was used as the positive and negative control for the cytotoxicity study in vitro under the same condition. The IC_{50} values (concentration

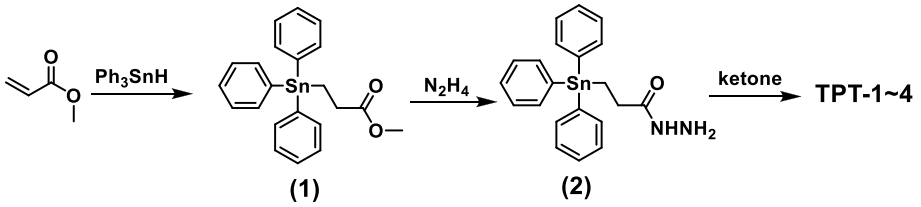

Scheme 1. Preparation of the triphenyltin(IV) compounds.

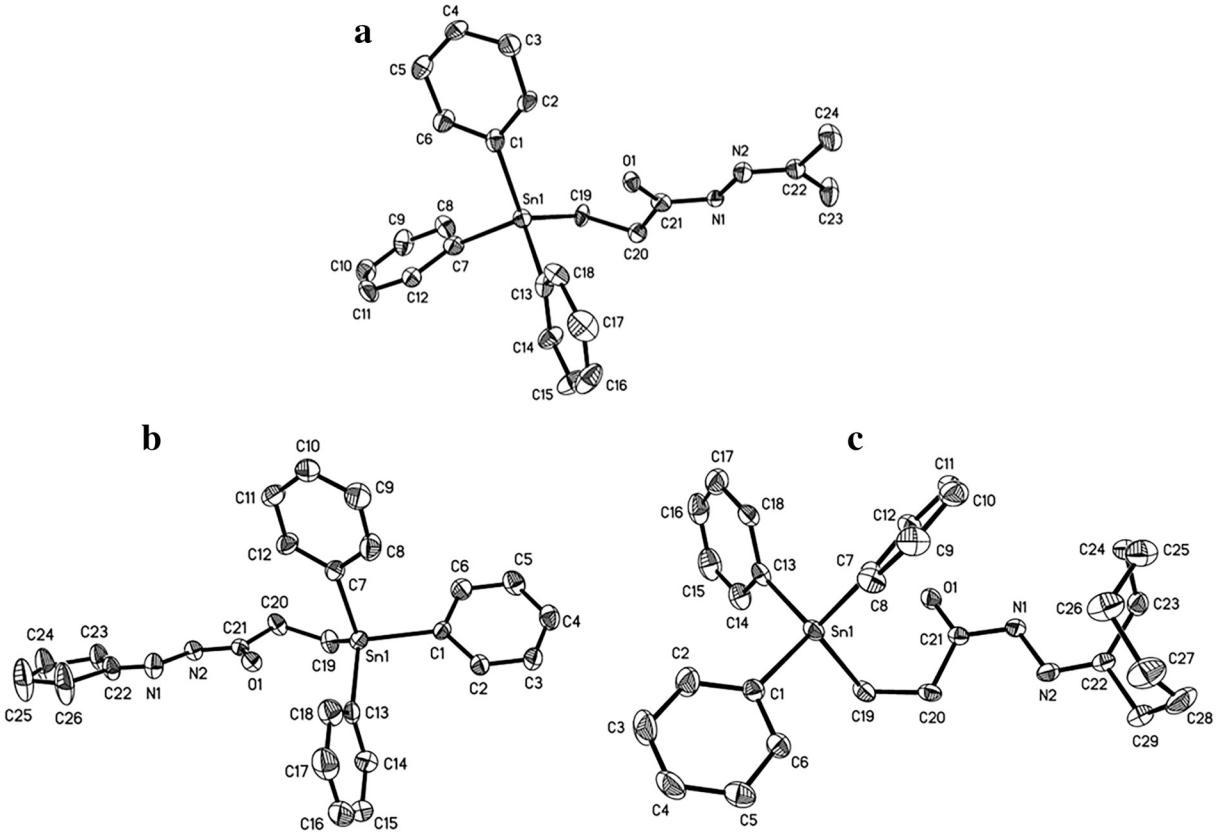

Fig. 2. The molecular structure of **TPT-1** (a), **TPT-3** (b) and **TPT-4** (c). The hydrogen atoms have been omitted for clarity.

at which 50% of the cell growth is inhibited) of exposure to tin(IV) compounds after 24 h were shown in Table 3. Compared with compound **2**, target triphenyltin(IV) compounds (**TPT-1–TPT-4**) exhibit the higher antitumor activity. **TPT-1** and **TPT-4** displayed the higher activities in vitro, which were more active than the clinically widely used *cis*-platin. The activity of **TPT-4** is the best, indicating the terminal substituent, large circle alkyl group seems to have a favorable effect on antitumor activity. Thus, further structure modification based on the acylhydrazone may modulate the cytotoxicity for these compounds.

The antiproliferative activities of **TPT-2** and **TPT-4** were further evaluated against two human bronchial epithelial normal cells (16HBE and BEAS-2B). As shown in Table 3, **TPT-2** and **TPT-4** show some selectivity for cancer cells versus normal cells, but it is not obvious. Therefore, more structural modification is necessary to improve the selectivity in future work.

2.3. Study of BSA interactions

It is necessary to understand what happened in cells by investigating the interaction between antitumor agents and protein [27]. In blood

Table 1
Crystal data and structure refinement for triphenyltin(IV) compounds.

	TPT-1	**TPT-3**	**TPT-4**
Empirical formula	$C_{24}H_{26}N_2OSn$	$C_{26}H_{28}N_2OSn$	$C_{29}H_{34}N_2OSn$
Formula weight	477.16	503.19	545.27
Temperature (K)	295(2)	295(2)	295(2)
Crystal system	Monoclinic	Monoclinic	Triclinic
Space group	*P* 21/*c*	*P* 21/*c*	*P*-1
a (Å)	10.970(3)	11.3898(10)	7.266(2)
b (Å)	15.136(8)	14.6174(12)	13.496(5)
c (Å)	30.02(3)	31.5542(19)	14.437(5)
volume (Å^3)	4693(5)	4917.4(7)	1372.1(8)
Z	8	8	2
D_c (g cm^{-3})	1.351	1.359	1.320
μ (mm^{-1})	1.104	1.057	0.953
F (000)	1936	2048	560
θ range (°)	1.44 to 25.25	1.38 to 26.00	1.42 to 26.00
crystal size (mm)	0.30 × 0.12 × 0.04	0.26 × 0.22 × 0.07	0.40 × 0.30 × 0.08
Tot. reflections	32,601	37,919	10,735
Uniq. reflections	8461 [R_{int} = 0.2484]	9639 [R_{int} = 0.1013]	5328 [R_{int} = 0.0532]
GOF on F^2	0.842	0.984	0.998
R indices [$I > 2\sigma(I)$]	R = 0.0748, wR = 0.1547	R = 0.0604, wR = 0.1137	R = 0.0572, wR = 0.1127
R indices (all data)	R = 0.2145, wR = 0.2022	R = 0.1257, wR = 0.1340	R = 0.0952, wR = 0.1265
$\triangle\rho_{min}$, $\triangle\rho_{max}$ (eÅ^{-3})	−0.642, 0.751	−0.409, 0.578	−0.513, 0.681

Table 2
Selected bond lengths (Å) and angles (deg.) for triphenyltin(IV) compounds.

	TPT-1	TPT-3	TPT-4
Sn(1)-C(1)	2.134(14)	2.161(6)	2.146(5)
Sn(1)-C(7)	2.136(13)	2.128(6)	2.138(5)
Sn(1)-C(13)	2.145(13)	2.129(7)	2.123(6)
Sn(1)-C(19)	2.144(11)	2.142(6)	2.141(5)
Sn(1)···O(1)	2.913(4)	2.855(3)	3.412(5)
C(1)-Sn(1)-C(7)	101.8(5)	103.8(2)	107.4(2)
C(1)-Sn(1)-C(13)	119.3(5)	103.7(2)	110.5(2)
C(1)-Sn(1)-C(19)	116.1(5)	105.0(2)	104.2(2)
C(7)-Sn(1)-C(13)	105.3(6)	112.3(3)	109.2(2)
C(7)-Sn(1)-C(19)	106.6(5)	113.3(3)	113.8(2)
C(13)-Sn(1)-C(19)	106.3(4)	117.0(3)	111.6(2)

plasma, serum albumin (SA) act the important role in drug transport and metabolism [28]. In this work, bovine serum albumin (BSA) was used to investigate the interaction with as-synthesized tin(IV) compounds for its structural similarity to human serum albumin (HSA), and also easily obtained.

The ultraviolet-visible (UV–vis) absorption spectra of BSA in the absence and presence of tin(IV) compounds are shown in Fig. 4a (**TPT-1**) and ESI Fig. S7 (**TPT-2–TPT-4**). As shown, the absorption peak decreased significantly and shifted towards longer wavelength at 218 nm along with increasing the concentration of tin(IV) compounds, which was attributed to the induced perturbation of BSA because of tin(IV) compounds [29,30]. Obvious red-shift was found at 218 nm attributing to the effect of the polar solvent (water) [31]. The binding of BSA to compounds was also reflected by the quenching at 278 nm, but without any shift, which indicate that triphenyltin(IV) compounds were mainly changing the microenvironment of BSA [32,33].

Fluorescence quenching is another effective method to study the interaction between compounds and proteins. As shown in Fig. 4b (ESI Fig. S8), with the increase of **TPT-1**, the fluorescence intensity of BSA decreases continuously at 343 nm [34]. To get a possible quenching mechanism, emission quenching data have been analyzed by the classical Stern–Volmer equation and Scatchard equation [35,36], and the important fitted data were listed in Table 4 (ESI Figs. S9 and S10). As shown, the quenching rate constant K_q for all compounds range from 2.74×10^{12} to $7.58 \times 10^{12}\,M^{-1}\,s^{-1}$, which are about two orders of magnitude higher than that of a purely dynamic quenching mechanism ($2.0 \times 10^{10}\,M^{-1}\,s^{-1}$), and indicating that a static quenching mechanism dominates in the interaction of tin(IV) compounds and BSA [37]. The binding site number **n** and binding constant K_b of all tin(IV) compounds were almost the same. But **TPT-4** show the bigger K_b ($5.52 \times 10^4\,M^{-1}$) compared with other tin(IV) compounds, which is consistent with the conclusion that **TPT-4** having the best antitumor activity.

2.4. Reaction with NADH

In many biological processes, reduced form of nicotinamide-adenine dinucleotid (NADH) play a major role [38]. Transition metal compound can oxidize NADH to NAD^+ and generate reactive oxygen species (ROS), which is the important oxidation antitumor mechanism [39]. The interaction between tin(IV) compounds and NADH can be detected at 259 nm and 340 nm by UV–vis spectrum (Fig. 5a and ESI Fig. S11). The absorption bands in 259 nm region can be assigned to the absorption of NAD^+ (produced by tin(IV) compounds capture hydrogen ions on NADH), while peaks at 340 nm are the absorption of NADH [40]. The turnover numbers (TONs) of **TPT-1** (7.18), **TPT-2** (2.15), **TPT-3** (6.17) and **TPT-4** (7.95) were calculated by measuring the difference at 340 nm (Fig. 5b). TONs show that all triphenyltin(IV) compounds can oxidize NADH to NAD^+. Among these, **TPT-4** shows the best activity, which are in accord with the results obtained in vitro cytotoxicity, and also demonstrating that the introduction of large cyclic alkanes is helpful to improve the catalytic performance of tin(IV) compound.

2.5. Apoptosis assay

TPT-2 and **TPT-4** are selected for more research on action mechanism. In order to evaluate whether the cell death caused by tin(IV) compounds is based on the mechanism of apoptosis, the annexin V assay was performed. A549 lung cancer cells were treated with **TPT-2** and **TPT-4** at 1, 2 and 3 × IC_{50} for 24 h, followed by staining with annexin V/propidium iodide (PI), and analyzed by flow cytometry. As shown in Fig. 6, cells in apoptosis stage increased with the concentration of tin(IV) compounds. **TPT-2** and **TPT-4** dramatically induce apoptosis during 24 h at a concentration of 3 × IC_{50}, with 36.6% and 47.5% cells undergoing apoptosis (early apoptosis + late apoptosis), respectively, compared with ~7% of control (ESI Tables S1 and S2).

2.6. Cell cycle analysis

Cell cycle arrest analysis for **TPT-2** and **TPT-4** against A549 lung cancer cells were investigated by flow cytometry. As shown in Fig. 7 (ESI Tables S3 and S4), the cell cycle progression was analyzed at 0.25, 0.5 and 1.0 equipotent concentrations of IC_{50} for 24 h. At a concentration of 1.0 × IC_{50}, compared with control, the percentages of cells in the S phase and G_1 phase increased from 25.0% and 10.2% to 43.9% and 21.1% when exposed to **TPT-2**. For **TPT-4**, at a concentration of 1.0 × IC_{50}, the percentages of cells in the S phase of the cell cycle increased from 22.6% to 36.1%. Compared with the untreated control, complex **TPT-4** disturbs the cell cycle at S and G_1 phase, while **TPT-2** mainly disturbing the cell cycle at S phase. The results indicate that these tin(IV) compounds can effectively disturb the cell growth cycle progression, and achieving the purpose of apoptosis.

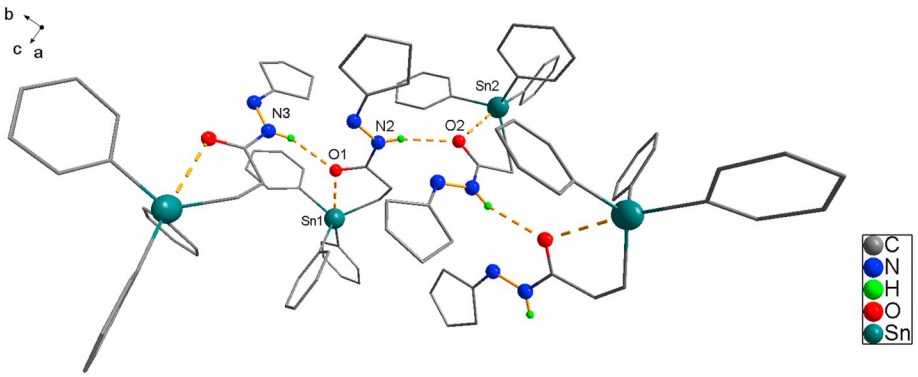

Fig. 3. The 1D chain structure of **TPT-3,** formed through intermolecular hydrogen bonds. All the hydrogen atoms are omitted for clarity except for forming intermolecular hydrogen bonds.

Table 3
IC_{50} values of compound **2**, **TPT-1–TPT-4** and *cis*-platin against A549 Cancer Cells and human bronchial epithelial normal cells after 24 h exposure.

Compounds	IC_{50} (μM) A549	IC_{50} (μM) 16HBE	IC_{50} (μM) BEAS-2B
2	> 100	–	–
TPT-1	16.0 ± 2.1	–	–
TPT-2	32.6 ± 0.52	72.1 ± 2.5	40.4 ± 0.3
TPT-3	23.9 ± 1.4	–	–
TPT-4	7.7 ± 0.5	30.3 ± 0.6	15.7 ± 3.0
cis-Platin	21.3 ± 1.7	–	–

2.7. Induction of ROS

Excessive production of reactive oxygen species (ROS) often led to oxidative stress and damages to cells [38]. The levels of ROS induced by **TPT-2** and **TPT-4** were investigated by flow cytometry analysis (Fig. 8, ESI Tables S5 and S6). A marked increase of ROS levels in A549 cells were observed after 24 h exposed to **TPT-2** and **TPT-4** even at a concentration of 0.25 × IC_{50}, around 75% of A549 cells were in high ROS levels. These observations are consistent with the proposed mechanism of action for **TPT-2** and **TPT-4**, which is based on the disruption of the cellular redox balance [41]. The significant increase of ROS levels may provide a basis for killing cancer cells.

3. Conclusion

In this study, four triphenyltin(IV) acylhydrazone compounds were synthesized with cheap starting materials and simple synthesis processes. The introduction of acylhydrazone group to the alkyl substituent increase the carbon chain length and the volume, meanwhile enhancing the lipid solubility and improving antitumor activity of tin(IV) compounds. **TPT-4** showed the best activity towards A549 lung cancer cells (IC_{50}: 7.7 ± 0.5 μM) and some selectivity. The UV–vis and PL test show all compounds can effectively bind with BSA, which indicate tin(IV) compounds can transport through blood plasma. Triphenyltin(IV) compounds can oxidize NADH to generate ROS and lead to apoptosis. The results of flow cytometry indicate that the compounds can disturb the cell growth cycle, which further confirmed the apoptosis mechanism. Above all, triphenyltin(IV) acylhydrazone compounds could be a promising candidate for further evaluation as antitumor drugs.

Table 4
The values of K_q, K_b and n for as-synthesized triphenyltin(IV) compounds.

Compounds	K_q ($10^{12}\,M^{-1}S^{-1}$)	K_b ($10^4\,M^{-1}$)	n
TPT-1	2.74	4.37	1.04
TPT-2	4.20	1.32	0.90
TPT-3	5.74	3.68	0.96
TPT-4	7.58	5.52	0.98

4. Experimental section

4.1. General

All chemicals were commercial grade and used without purification. Triphenyltin chloride, Lithium Aluminum Hydride, methyl acrylate, hydrazine hydrate (80%), acetone, butanone, cyclopentanone, Cyclooctanone and other organic reagents were purchased from Shanghai Pengteng Fine Chemical Co., Ltd. For the biological experiments, DMEM medium, fetal bovine serum, reduced form of nicotinamide-adenine dinucleotid (NADH) were purchased from Sangon Biotech. A549 lung cancer cells were obtained from Shanghai Institute of Biochemistry and Cell Biology (SIBCB). Carbon, hydrogen, oxygen and nitrogen analyses were performed using a Perkin Elmer 2400 Series II elemental analyzer (Perkin Elmer, Waltham, MA, USA). IR spectra were recorded on a Nicolet Nexus 470 FT-IR spectrophotometer using KBr discs in the range 4000–400 cm^{-1} (Thermo Nicolet Corporation, Madison, WI, USA). ^1H and ^{13}C NMR spectral data were collected using a Bruker Avance DPX 500 with $CDCl_3$ as the solvent and tetramethylsilane (TMS) as the internal standard, and tetramethyltin ($SnMe_4$) as external standard for ^{119}Sn NMR using a Bruker Avance DPX300 NMR spectrometer. Intensity data for the crystals were measured at 295(2) K on a Bruker Smart Apex area-detector fitted with graphite monochromatized Mo-*K*α radiation (0.71073 Å) using the φ and ω scan technique. UV–vis spectroscopy was performed on a TU-1901 UV spectrometer. The fluorescence spectra were collected by a fluorescence spectrophotometer (F-4600, Hitachi) with a 400 V voltage and 5 nm slit width for both excitation and emission. Apoptosis and ROS determination were carried out using the Annexin V-FITC Apoptosis Detection Kit (Beyotime Institute of Biotechnology, China). MTT assay were measured using a microplate reader (DNM-9606, Perlong Medical, Beijing, China) at an absorbance of 570 nm.

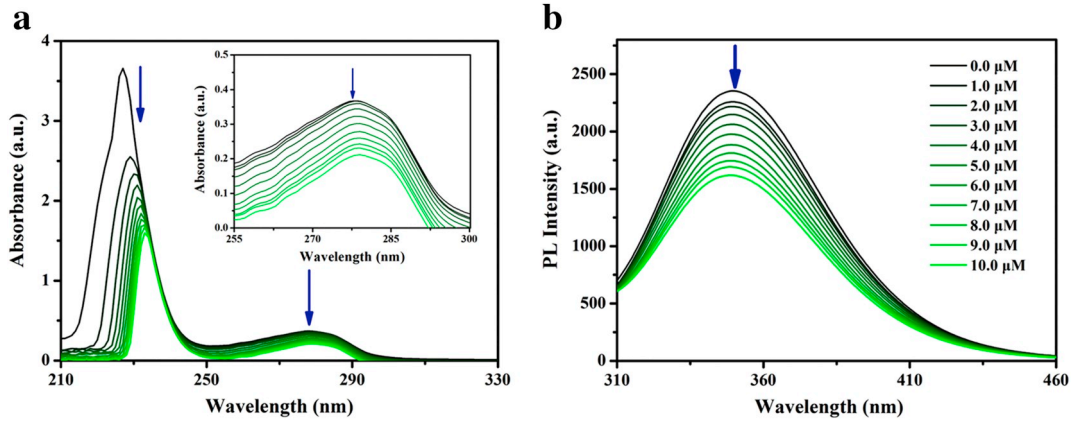

Fig. 4. (a) UV–vis spectrum of BSA in 5 mM Tris–HCl/10 mM NaCl buffer solution (pH = 7.2) upon addition of **TPT-1** (0–10.0 μM). The arrows show the direction of changes in absorbance upon increasing the concentration of **TPT-1**. Inset: wavelength from 255 to 300 nm. (b) Fluorescence spectra of BSA (0.5 μM; λ_{ex} = 280 nm; λ_{em} = 343 nm) in the absence and presence of the **TPT-1** (0–10.0 μM).

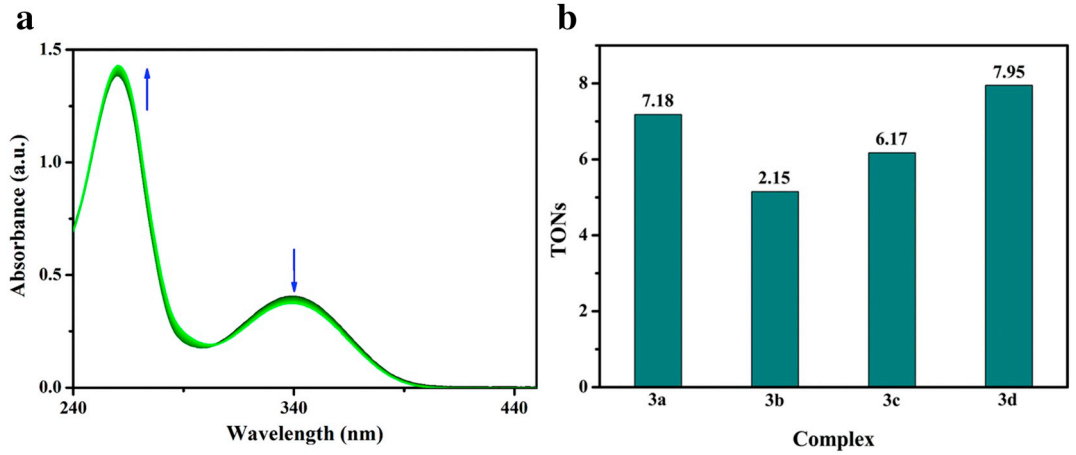

Fig. 5. (**a**) UV–vis spectra of the reaction of NADH (100 μM) with **TPT-1** (1 μM) in 10% MeOH/90% H_2O (V:V) at 298 K for 8 h. The arrows show changes in absorbance spectra over time; (**b**) The TONs of as-synthesized triphenyltin(IV) compounds.

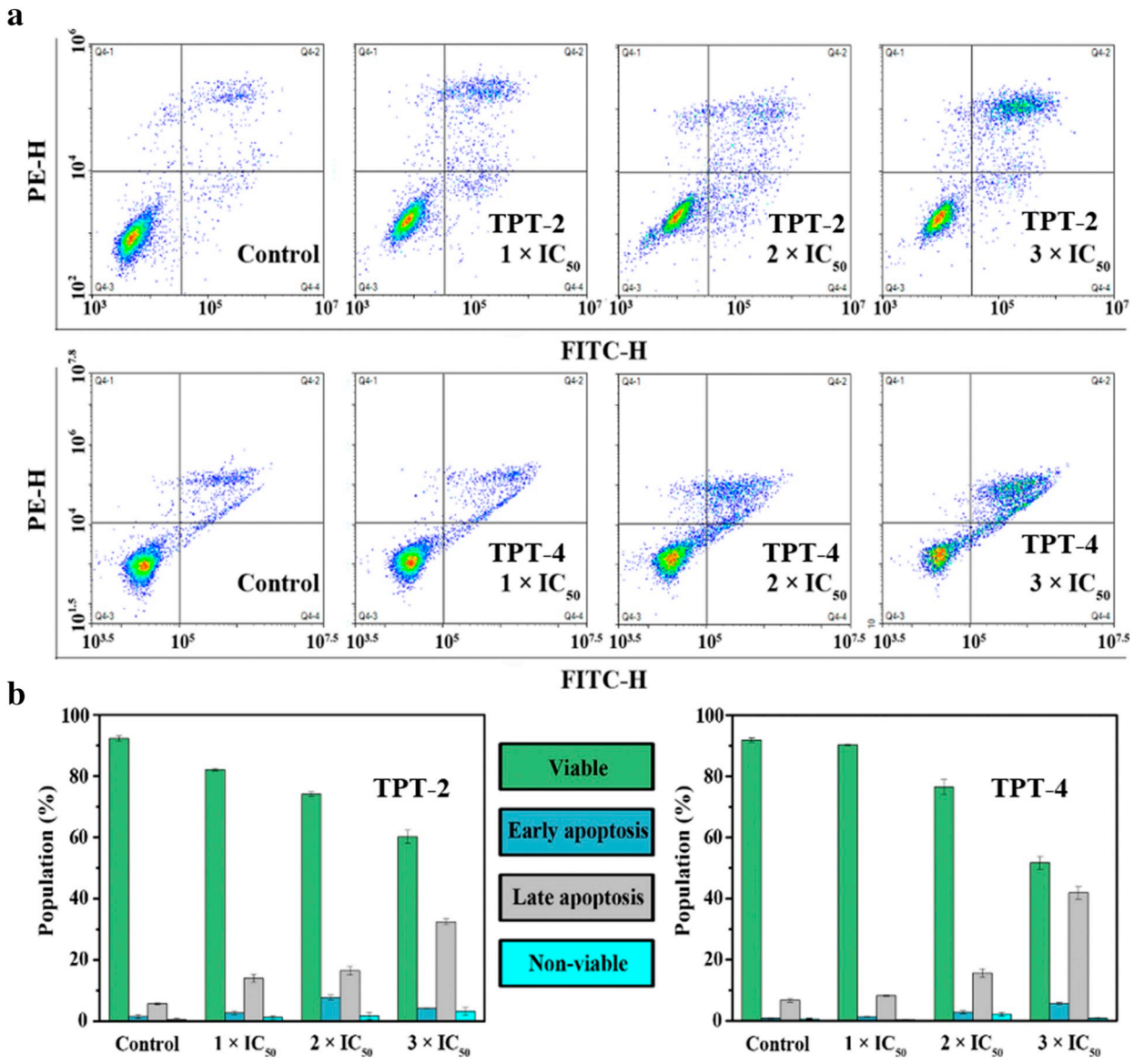

Fig. 6. (a) Apoptosis induction detected by annexin V-FITC and PI staining and flow cytometry analysis in A549 cells after 24 h of exposure to **TPT-2** and **TPT-4** at various concentrations at 310 K. (b) Histogram showing populations for A549 cells in four stages treated by **TPT-2** and **TPT-4**. Data are quoted as mean ± SD of three replicates.

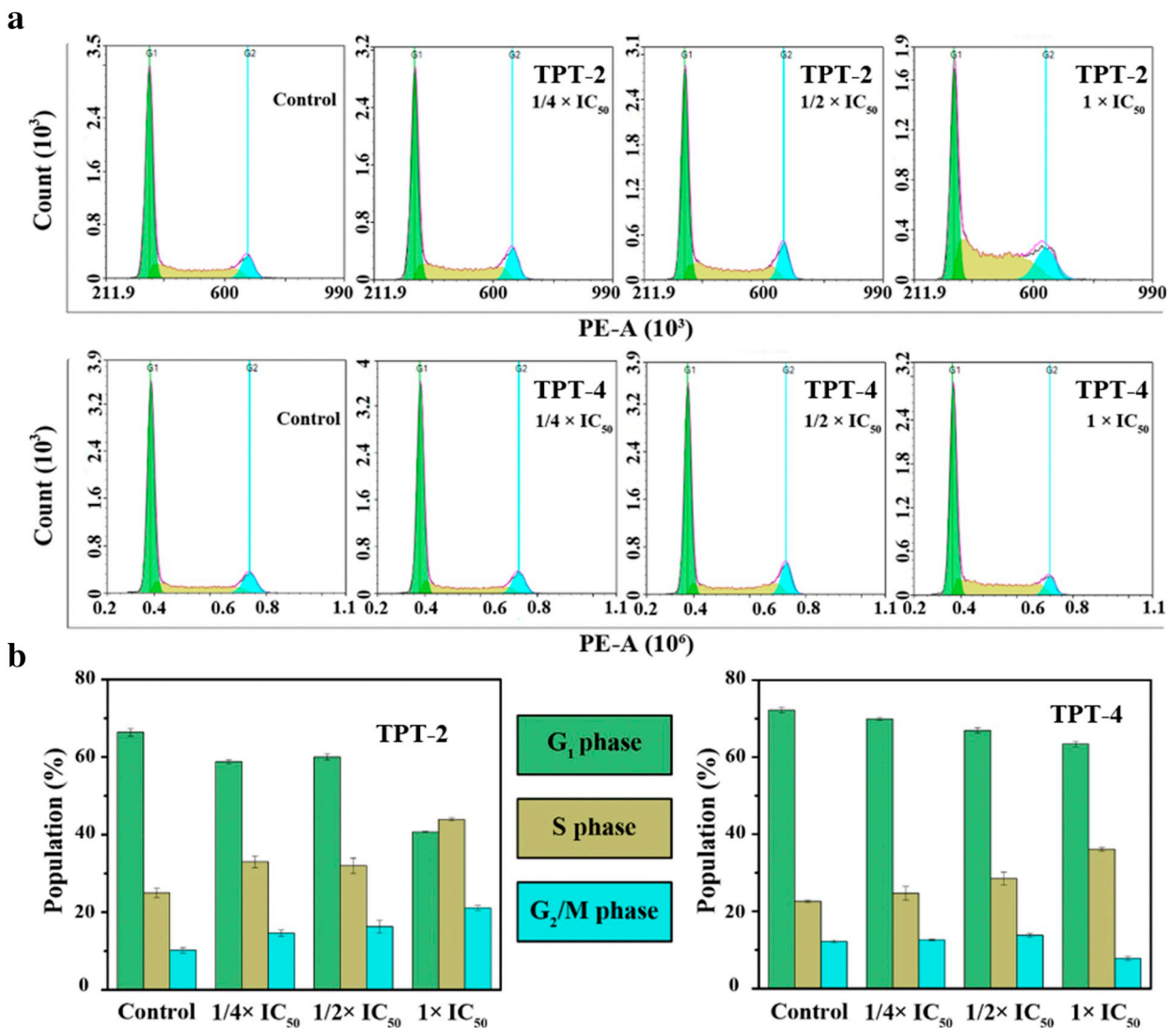

Fig. 7. (a) Cell cycle analysis of A549 lung cancer cells after 24 h of exposure to **TPT-2** and **TPT-4** at the indicated concentrations by flow cytometry using PI staining. (b) Populations in each cell cycle phase for control, **TPT-2** and **TPT-4.**

4.2. Synthesis

4.2.1. Synthesis of β-methoxycarbonyl ethyl triphenyltin(IV) ***(1)***

Compound **1** was prepared according to literature methods [42]. Under the protection of N_2, methyl acrylate (5.2 g, 0.06 mol), azodiisobutyronitrile (AIBN, 0.3 g, 2.0 mmol) and triphenyl hydrogenated tin (17.6 g, 0.05 mol) were added to 150 mL anhydrous ether solution. At the same time, a small amount of hydroquinone was added, which was stirred under ultrasonic radiation for 4 h, decompressed and steamed to remove the solvent, and a colorless viscous substance was obtained. Yield: 75.9%, Mp, 46.1–47.3 °C; ^{1}H NMR (500 MHz, $CDCl_3$)/δ: 7.54–7.56 (m, 6H, $J(^{119}$Sn-H) = 47.5 Hz, *o*-H in C_6H_5), 7.36–7.38 (m, 9H, *m*- and *p*-H of Ph), 3.47 (s, 3H, OCH_3), 2.68 (t, J = 7.8 Hz, 2H, $J(^{119}$Sn-H) = 67.1 Hz, CH_2CO), 1.67 (t, J = 7.8 Hz, 2H, $J(^{119/117}$Sn-^{1}H) = 55.1/52.9 Hz, CH_2Sn).

4.2.2. Synthesis of β-hydrazinocarbonyl ethyl triphenyltin(IV) ***(2)***

Compound **1** (2.0 g, 4.5 mmol) and methanol (30 mL) were added into a 250 mL three-necked bottle under N_2, followed by stirring and heating to ebullience for 20 min. Hydrazine hydrate (50%, 30 mL) was added dropwise to above solution at 80 °C. The reaction stopped until compound **1** was consumed completely (monitored by thin-layer chromatography). Crude product was isolated by filtration, and recrystallized from 60 mL mixture of chloroform and petroleum ether (V/V = 1:1) to obtain acicular colorless crystal. Yield: 80.1%; Mp, 144.2–144.5 °C; selected IR (KBr): 1680 cm^{-1} (C═O); ^{1}H NMR (500 MHz, $CDCl_3$) δ 7.64–7.50 (m, 6H, $^3J(^{119}$Sn-H) = 45.0 Hz, o-H of Ph), 7.42–7.33 (m, 9H, *m*- and *p*-H of Ph), 2.60–2.39 (t, J = 7.8 Hz, 2H, $^3J(^{119}$Sn-H) = 67.3 Hz, CH_2CO), 1.76–1.60 (t, J = 7.8 Hz, 2H, $^2J(^{119}$Sn-H) = 53.6 Hz, CH_2Sn); ESI-MS (*m/z*): $[M + Na]^+$ Calcd for $C_{21}H_{22}N_2OSn$, 461.08; Found 461.25.

4.2.3. Synthesis of β-acylhydrazone ethyl triphenyltin(IV) ***(TPT)***

Compound **2** (1 eq) and corresponding ketone (1 eq) were mixed in round-bottom flask, and adding chloroform as the reaction solvent. The mixture was stirred at 80 °C until compound **2** was consumed completely (monitored by thin-layer chromatography). After rotary evaporation, the crude product was recrystallized from the mixture of chloroform and petroleum ether (V/V = 1:1). The characterization data were described for each case as follows:

$Ph_3SnCH_2CH_2CONHN{=}C(CH_3)_2$ (TPT-1): Colorless crystal; Yield: 87.3%; Mp, 134.9–136.5 °C; selected IR (KBr): 3228 (N-H), 3060 (Ph-H), 3042, 2987 (C-H), 1661 (C═O) 1548, 1480, 1428 (C═C, Ph), 727, 698 (C-H, Ph), 450 (Sn-C) cm^{-1}; ^{1}H NMR (500 MHz, $CDCl_3$) δ 8.66 (s, 1H, NH), 7.74 (dd, J = 7.5, 1.5 Hz, 6H, $^3J(^{119}$Sn-H) = 59.5 Hz, o-H of Ph), 7.45–7.29 (m, 9H, *m*- and *p*-H of Ph), 3.17 (t, J = 7.7 Hz, 2H, ^3J

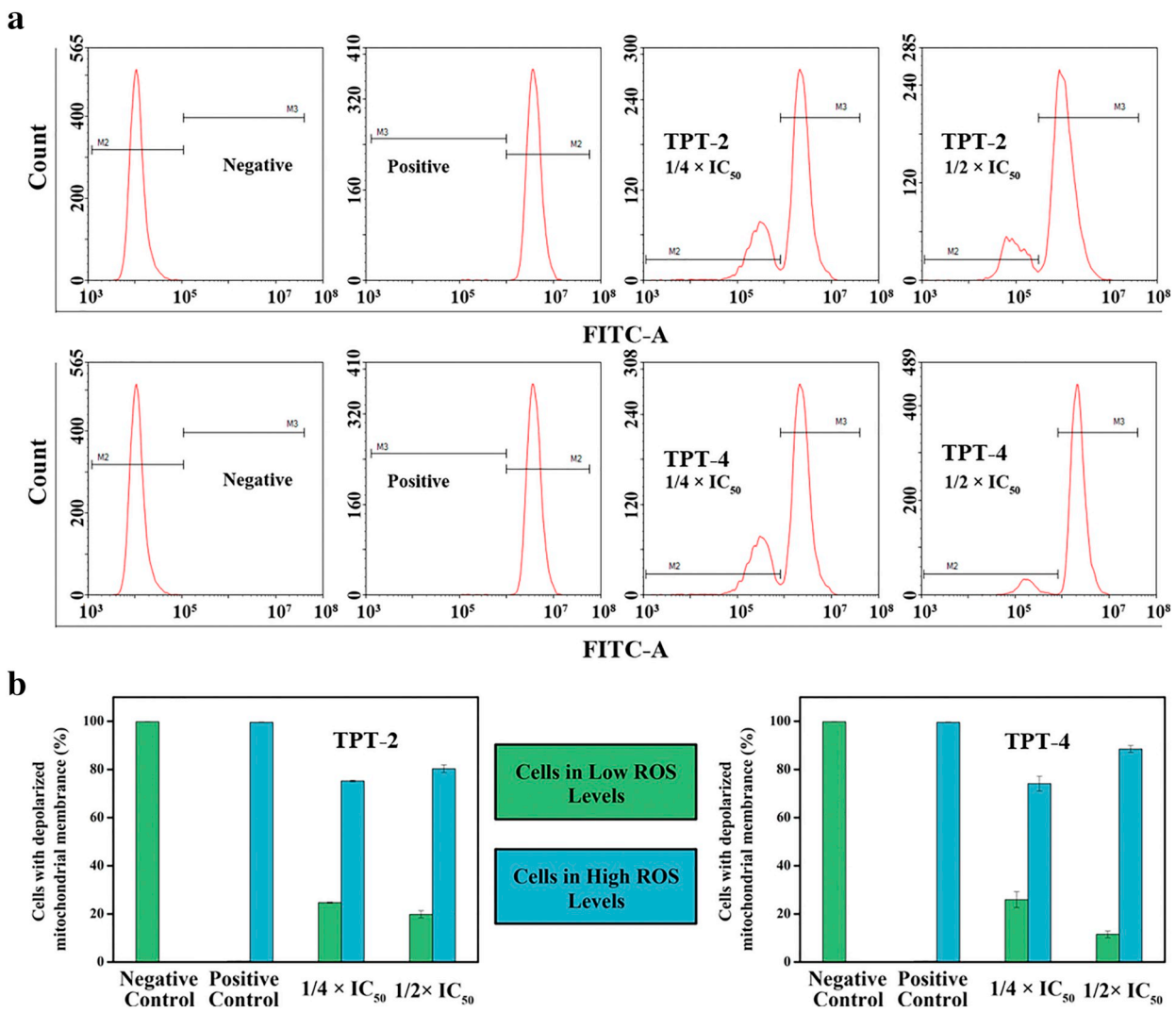

Fig. 8. ROS induction in A549 cancer cells caused by **TPT-2** and **TPT-4** at concentration of 0.25 and 0.50 × IC_{50}. (a) FL2 histogram for negative control (cells untreated), positive control, **TPT-2** and **TPT-4**. (b) Populations of cells in low and high level of ROS after treatment of **TPT-2** and **TPT-4.** Data are quoted as mean ± SD of three replicates.

(^{119}Sn-H) = 101.5 Hz, CH_2CO), 2.01 (s, 3H, CH_3CN), 1.81 (s, 3H, CH_3CN), 1.75 (dd, J = 12.6, 4.8 Hz, 2H, $SnCH_2$); ^{13}C NMR (126 MHz, $CDCl_3$) δ 176.37 (C═O), 148.75 (C═N), 139.86 (^1J (^{119}Sn-^{13}C) = 496 Hz, C-*i* of PhSn), 137.15 (^2J(^{119}Sn-^{13}C) = 35.5 Hz, C-*o* of PhSn), 128.70 (^4J(^{119}Sn-^{13}C) = 12 Hz, C-*p* of PhSn), 128.29 (^3J (^{119}Sn-^{13}C) = 49 Hz, C-*m* of PhSn), 29.09 (^2J(^{119}Sn-^{13}C) = 23 Hz, C*-CO), 25.31 (C*-CN), 15.74 (C*-CN), 5.37 (CH_2-Sn); ^{119}Sn NMR (112 MHz, $CDCl_3$) δ: −130.38; Elemental analysis: Found: C 61.09, H 5.78, N 5.65, O 3.30%, anal. Calcd. for $C_{25}H_{28}N_2OSn$: C 61.15, H 5.75, N 5.60, O 3.24%. ESI-MS (*m/z*): $[M + Na]^+$ Calcd for $C_{24}H_{26}N_2OSn$, 501.11; Found 501.33.

$Ph_3SnCH_2CH_2CONHN{=}C(CH_3)(C_2H_5)$ (TPT-2): Colorless crystal; Yield: 80.6%; Mp, 129.3–130.5 °C; selected IR (KBr): 3229 (N-H), 3059 (Ph-H), 2962, 2905 (C-H), 1660 (C═O) 1548, 1480, 1428 (C═C, Ph), 727, 699 (C-H, Ph), 451 (Sn-C) cm^{-1}; ^{1}H NMR (500 MHz, $CDCl_3$) δ 8.05 (s, 1H, NH), 7.66–7.50 (m, 6H, ^{3}J(^{119}Sn-H) = 45.0 Hz, o-H of Ph), 7.40–7.28 (m, 9H, *m*- and *p*-H of Ph), 3.04 (dd, J = 9.5, 6.1 Hz, 2H, ^3J (^{119}Sn-H) = 68.0 Hz, CH_2CO), 2.22 (q, J = 7.4 Hz, 2H, CH_2-CN), 1.78–1.48 (m, 5H, $SnCH_2$ and CH_3CN), 1.03 (t, J = 7.3 Hz, 3H, CH_3CH_2); ^{13}C NMR (126 MHz, $CDCl_3$) δ 176.63 (C═O), 152.55 (C═N), 139.79 (^1J(^{119}Sn-^{13}C) = 501 Hz, C-*i* of PhSn), 137.16 (^2J (^{119}Sn-^{13}C) = 35.5 Hz, C-*o* of PhSn), 128.61 (^4J(^{119}Sn-^{13}C) = 11.5 Hz, C-*p* of PhSn), 128.31 (^3J(^{119}Sn-^{13}C) = 49.0 Hz, C-*m* of PhSn), 32.02 (CH_2 of 2-Butyl), 29.18 (^2J(^{119}Sn-^{13}C) = 23.8 Hz, C*-CO), 14.61 (CH_3 of 2-Butyl), 10.40 (CH_3 of 2-Butyl), 5.33 (CH_2-Sn); ^{119}Sn NMR (112 MHz, $CDCl_3$) δ: −101.77; Elemental analysis: Found: C 61.18, H 5.69, N 5.68, O 3.25%, anal. calcd. for $C_{25}H_{28}N_2OSn$: C 61.24, H 5.77, N 5.60, O 3.17%. ESI-MS (*m/z*): $[M + Na]^+$ Calcd for $C_{25}H_{28}N_2OSn$, 515.12; Found 515.33.

$Ph_3SnCH_2CH_2CONHN{=}CC_4H_8$ (TPT-3): Colorless crystal; Yield: 81.6%; Mp, 146.3–147.6 °C; selected IR (KBr): 3229 (N-H), 3059 (Ph-H), 2970, 2908 (C-H), 1660 (C═O) 1548, 1480, 1427 (C═C, Ph), 727, 699 (C-H, Ph), 451 (Sn-C) cm^{-1}; ^{1}H NMR (500 MHz, $CDCl_3$) δ 7.82 (s, 1H, NH), 7.67–7.50 (m, 6H, ^{3}J(^{119}Sn-H) = 45.5 Hz, o-H of Ph), 7.41–7.28 (m, 9H, *m*- and *p*-H of Ph), 3.02 (t, J = 7.6 Hz, 2H, ^3J(^{119}Sn-H) = 71.5 Hz, CH_2CO), 2.33 (t, J = 7.2 Hz, 2H, CH_2-CN), 2.03 (t, J = 7.1 Hz, 2H, CH_2-CN), 1.85–1.66 (m, 6H, $SnCH_2$ and CH_2CH_2 of cyclopentyl); ^{13}C NMR (126 MHz, $CDCl_3$) δ 176.22 (C═O), 161.94 (C═N), 139.93 (^1J(^{119}Sn-^{13}C) = 502 Hz, C-*i* of PhSn), 137.17 (^2J (^{119}Sn-^{13}C) = 35 Hz, C-*o* of PhSn), 128.60 (^4J(^{119}Sn-^{13}C) = 11 Hz, C-*p* of PhSn), 128.30 (^3J(^{119}Sn-^{13}C) = 48 Hz, C-*m* of PhSn), 33.23 (CH_2 of cyclopentyl), 29.02 (^2J(^{119}Sn-^{13}C) = 24 Hz, CH_2-CO), 26.89 (CH_2 of cyclopentyl l), 24.82 (CH_2 of cyclopentyl), 24.73 (CH_2 of cyclopentyl), 5.44 (CH_2-Sn); ^{119}Sn NMR (112 MHz, $CDCl_3$) δ: −102.43; Elemental analysis: Found: C 62.11, H 5.59, N 5.61, O 3.21%, anal.calcd for $C_{26}H_{28}N_2OSn$: C 62.18, H 5.63, N 5.57, O 3.17%. ESI-MS (*m/z*):

$[M + Na]^+$ Calcd for $C_{26}H_{28}N_2OSn$, 527.12; Found 527.33.

$Ph_3SnCH_2CH_2CONHN{=}CC_7H_{12}$ (TPT-4): Colorless crystal; Yield: 78.2%; Mp, 94.3–94.7 °C; selected IR (KBr): 3187 (N-H), 3062 (Ph-H), 2929, 2854 (C-H), 1667 (C═O) 1577, 1480, 1463, 1427 (C═C, Ph), 727, 698 (C-H, Ph), 453 (Sn-C) cm^{-1};^{1}H NMR (500 MHz, $CDCl_3$) δ 8.14 (d, J = 10.5 Hz, 1H, NH), 7.68–7.50 (m, 6H, $^3J(^{119}Sn\text{-}H)$ = 46 Hz, o-H of Ph), 7.43–7.30 (d, J = 3.7 Hz, 9H m- and p-H of Ph), 3.03 (t, J = 7.7 Hz, 2H, $^3J(^{119}Sn\text{-}H)$ = 71 Hz, CH_2CO), 2.33–2.24 (m, 2H, CH_2-CN), 2.23–2.10 (m, 2H, CH_2-CN), 1.71 (ddd, J = 18.4, 13.7, 8.1 Hz, 4H, $SnCH_2$ and CH_2 of cyclooctyl), 1.62 (dt, J = 12.1, 6.1 Hz, 2H, CH_2 of cyclooctyl), 1.48 (ddd, J = 22.3, 11.8, 6.7 Hz, 4H, CH_2CH_2 of cyclooctyl), 1.42–1.32 (m, 2H, CH_2 of cyclooctyl); ^{13}C NMR (126 MHz, $CDCl_3$) δ 176.47 (C═O), 157.90 (C═N), 139.93 ($^1J(^{119}Sn\text{-}^{13}C)$ = 500 Hz, C-i of PhSn), 137.17 ($^2J(^{119}Sn\text{-}^{13}C)$ = 35.5 Hz, C-o of PhSn), 128.59 ($^4J(^{119}Sn\text{-}^{13}C)$ = 11 Hz, C-p of PhSn), 128.29 ($^3J(^{119}Sn\text{-}^{13}C)$ = 48 Hz, C-m of PhSn), 36.60 (CH_2 of cyclooctyl), 29.22 ($^2J(^{119}Sn\text{-}^{13}C)$ = 23.5 Hz, CH_2-CO), 27.38 (CH_2 of cyclooctyl), 27.08 (CH_2 of cyclooctyl), 26.24 (CH_2 of cyclooctyl), 25.33 (CH_2 of cyclooctyl), 24.42 (CH_2 of cyclooctyl), 24.38 (CH_2 of cyclooctyl), 5.40 (CH_2-Sn); ^{119}Sn NMR (112 MHz, $CDCl_3$) δ: −102.01; Elemental analysis: Found: C 63.91, H 6.26, N 5.12, O 2.92%, anal.calcd for $C_{29}H_{34}N_2OSn$: C 63.97, H 6.29, N 5.08, O 2.87%. ESI-MS (m/z): $[M + Na]^+$ Calcd for $C_{29}H_{34}N_2OSn$, 569.17; Found 569.42.

Abbreviations

TPT	Triphenyltin
SA	Serum Albumin
HSA	Human Serum Albumin
BSA	Bovine Serum Albumin
ROS	Reactive Oxygen Species
Ph	Phenyl
NADH	Nicotinamide Adenine Dinucleotide
IC_{50}	Concentration at Which 50% of theCell Growth is Inhibited
TONs	Turnover Numbers
MTT	Thiazolyl Blue Tetrazolium Bromide

Acknowledgments

We thank Student's Platform for Innovation and Entrepreneurship Training Program of Shandong Province (201710446042), the University Research Development Program of Shandong Province (J18KA082), the National Natural Science Foundation of China (Grant No. 21671118) and the Taishan Scholar Project of Shandong Province for support.

Notes

The authors declare no competing financial interest.

Appendix A. Supplementary data

Supplementary data to this article can be found online at https://doi.org/10.1016/j.jinorgbio.2018.11.011.

References

[1] B. Rosenberg, L. Vancamp, J.E. Trosko, V.H. Mansour, Nature 222 (1969) 385–386.
[2] X.D. He, X.C. Liu, Y.H. Tang, J.Y. Du, M. Tian, Z.S. Xu, X.Y. Liu, Z. Liu, Dyes Pigments 160 (2019) 217–226.
[3] Y.L. Han, Z.Z. Tian, S.M. Zhang, X.C. Liu, J.J. Li, Y.R. Liu, Y. Liu, M. Gao, Z. Liu, J. Inorg. Biochem. 189 (2018) 163–171.
[4] X.Z. Xu, D.L. Kong, X.D. He, L.H. Guo, X.X. Ge, X.C. Liu, H.R. Hai, J.J. Li, Y.L. Yang, Z. Liu, Inorg. Chem. Front. 5 (2018) 2100–2105.
[5] X. Wang, Z. Guo, Chem. Soc. Rev. 42 (2013) 202–224.
[6] A.A. Argyriou, P. Polychronopoulos, G. Iconomou, E. Chroni, H.P. Kalofonos, Cancer Treat. Rev. 34 (2008) 368–377.
[7] G. Gasser, I. Ott, N. Metzler-Nolte, J. Med. Chem. 54 (2011) 3–25.
[8] Y.Z. Yao, M. Yang, X.L. Zheng, L.J. Tian, Main Group Met. Chem. 40 (2017) 93–99.
[9] S.K. Hadjikakou, N. Hadjiliadis, Coord. Chem. Rev. 253 (2009) 235–249.
[10] A. Attanzio, M. Ippolito, M.Z. Girasolo, F. Saiano, A. Rotondo, S. Rubino, L. Mondello, M.L. Capobianco, P. Sabatino, L. Tesoriere, G. Casella, J. Inorg. Biochem. (2018), https://doi.org/10.1016/j.jinorgbio.2018.04.006.
[11] L.J. Tian, L. Han, Y.Z. Yao, X.F. Zheng, X. Liu, X. Lin, Appl. Organomet. Chem. 32 (2018) e4475.
[12] S. Hazra, A. Paul, G. Sharma, B. Koch, M.F.C.G. da Silva, A.J.L. Pombeiro, J. Inorg. Biochem. 162 (2016) 83–95.
[13] L.J. Tian, H.X. Yu, X.L. Zheng, X.J. Liu, Appl. Organomet. Chem. 29 (2015) 725–729.
[14] M. Nath, P.K. Saini, Dalton Trans. 40 (2011) 7077–7121.
[15] R. Pignatello, A. Panico, P. Mazzone, M.R. Pinizzotto, A. Garozzo, P.M. Furneri, Eur. J. Med. Chem. 29 (1994) 781–785.
[16] M.B. Bastos, J.C. Moreira, P.A. Farias, Anal. Chim. Acta 408 (2000) 83–88.
[17] S. Arulmurugan, H.P. Kavitha, R.P. Venkatraman, Rasayan J. Chem. 3 (2010) 385–410.
[18] Q.F. Xie, C.X. Lin, C.X. Liu, H.Q. Lu, X.L. Wu, Chem. Res. 27 (2016) 88–91.
[19] A. G. Davies, M. Gielen, K. H. Pannell, E. R. T. Tiekink, John Wiley& Sons, Chichester, U.K., 2008. DOI:https://doi.org/10.1002/9780470758090.
[20] S.S. Wang, L. Feng, J. Saf. Environ. 5 (2005) 12–15.
[21] J. Crown, P.J. Smith, G. Atassi, Chem. Biol. Interact. 32 (1980) 171–178.
[22] P. Harston, R.A. Howie, G.P. Mcquilan, J.L. Wardell, E. Zanetti, M.S.V. Solange, D. Harrison, N.S. Stewart, P.J. Cox, Polyhedron 10 (1991) 1085–1090.
[23] S. Durand, K. Sakamoto, T. Fukuyama, A. Orita, J. Otera, A. Duthie, D. Daktarnieks, M. Schulte, K. Jurkschat, Organometallics 19 (2000) 3220–3223.
[24] J. Holecek, M. Nadvornik, K. Handlir, A. Lycka, J. Organomet. Chem. 241 (1983) 177–184.
[25] L.J. Tian, Y.Z. Yao, Y.H. Wang, J. Liu, J. Mol. Struct. 1156 (2018) 441–449.
[26] S.A. Zhang, W.Q. Wang, Q.T. Liu, X.F. Zheng, L.J. Tian, Main Group Met. Chem. 39 (2016) 87–92.
[27] S.M. Meier, M.S.D. Kreutz, L. Winter, M.S.M.H.M. Kolse, M.S.K. Cseh, M.S.T. Weiss, A. Bileck, M.S.B. Alte, J.C. Mader, M.S.S. Jana, A. Chatterjee, A. Bhattacharyya, M. Hejl, M.A. Jakupec, W. Bergr, C.G. Hartinger, B.K. Keppler, G. Wiche, C. Gerner, Angew. Chem. Int. Ed. 56 (2017) 8267–8271.
[28] R. Esteghamat-Panah, H. Hadadzadeh, H. Farrokhpour, M. Mortazavi, Z. Amirghofran, Inorg. Chim. Acta 454 (2017) 184–196.
[29] C.L. Wang, J.F. Liu, Z.Z. Tian, M. Tian, L.J. Tian, W.Q. Zhao, Z. Liu, Dalton Trans. 46 (2017) 6870–6883.
[30] J.J. Li, L.H. Guo, Z.Z. Tian, M. Tian, S.M. Zhang, K. Xu, Y.C. Qian, Z. Liu, Dalton Trans. 46 (2017) 15520–15534.
[31] B.K. Paul, N. Guchhait, Photochem. Photobiol. Sci. 10 (2011) 980–991.
[32] J.J. Li, M. Tian, Z.Z. Tian, S.M. Zhang, C. Yan, C.F. Shao, Z. Liu, Inorg. Chem. 57 (2018) 1705–1716.
[33] X.D. He, M. Tian, X.C. Liu, Y.H. Tang, C.F. Shao, P.W. Gong, J.F. Liu, S.M. Zhang, L.H. Guo, Z. Liu, Chem. Asian J. 13 (2018) 1500–1509.
[34] R.D. Senthil, N.S. Bhuvanesh, K. Natarajan, Eur. J. Med. Chem. 46 (2011) 4584–4594.
[35] S. Mukhopadhyay, R.K. Gupta, R.P. Paitandi, N.K. Rana, G. Sharma, B. Koch, L.K. Rana, M.S. Hundal, D.S. Pandey, Organometallics 34 (2015) 4491–4506.
[36] R. Pettinari, F. Marchetti, A. Petrini, C. Pettinari, G. Lupidi, B. Fernández, A.R. Diéguez, G. Santoni, M. Nabissi, Inorg. Chim. Acta 454 (2016) 139–148.
[37] S. Chatterjee, T.K. Mukherjee, Phys. Chem. Chem. Phys. 16 (2014) 8400–8408.
[38] Z. Liu, I. Romerocanelón, B. Qamar, J.M. Hearn, A. Habtemariam, N.P. Barry, A.M. Pizarro, G.J. Clarkson, P.J. Sadler, Angew. Chem. Int. Ed. 53 (2014) 3941–3946.
[39] Z. Liu, R.J. Deeth, J.S. Butler, H. Abraha, M.E. Newton, P.J. Sadler, Angew. Chem. Int. Ed. 52 (2013) 4194–4197.
[40] B.L. Soledad, L. Zhe, H. Abraha, A.M. Pizarro, Q. Bushra, P.J. Sadler, Angew. Chem. Int. Ed. 124 (2012) 3963–3966.
[41] I. Romero-Canelón, M. Mos, P.J. Sadler, J. Med. Chem. 58 (2015) 7874–7880.
[42] L. Verdonck, G.P. van der Kelen, J. Organomet. Chem. 11 (1968) 491–497.